ARTICLES
https://doi.org/10.1038/s41587-021-01180-3
nature biotechnology

Engineered circular ADAR-recruiting RNAs increase the efficiency and fidelity of RNA editing in vitro and in vivo

Zongyi Yi[1,2,4], Liang Qu[1,4], Huixian Tang[1,4], Zhiheng Liu[1], Ying Liu[1], Feng Tian[1], Chunhui Wang[1], Xiaoxue Zhang[1,2], Ziqi Feng[1], Ying Yu[1], Pengfei Yuan[3], Zexuan Yi[3], Yanxia Zhao[3] and Wensheng Wei[1]✉

Current methods for programmed RNA editing using endogenous ADAR enzymes and engineered ADAR-recruiting RNAs (arRNAs) suffer from low efficiency and bystander off-target editing. Here, we describe LEAPER 2.0, an updated version of LEAPER that uses covalently closed circular arRNAs, termed circ-arRNAs. We demonstrate on average ~3.1-fold higher editing efficiency than their linear counterparts when expressed in cells or delivered as in vitro-transcribed circular RNA oligonucleotides. To lower off-target editing we deleted pairings of uridines with off-target adenosines, which almost completely eliminated bystander off-target adenosine editing. Engineered circ-arRNAs enhanced the efficiency and fidelity of editing endogenous *CTNNB1* and mutant *TP53* transcripts in cell culture. Delivery of circ-arRNAs using adeno-associated virus in a mouse model of Hurler syndrome corrected the pathogenic point mutation and restored α-L-iduronidase catalytic activity, lowering glycosaminoglycan accumulation in the liver. LEAPER 2.0 provides a new design of arRNA that enables more precise, efficient RNA editing with broad applicability for therapy and basic research.

Genome editing tools, such as zinc finger nucleases, transcription activator-like effector nucleases, the CRISPR–Cas system and CRISPR–Cas derivatives (cytosine and adenosine base editors), have been widely applied in manipulation of the genome, revealing their therapeutic potential. In addition to genome editing technologies, RNA base editing technologies have also been developed[1]. Because RNA editing is reversible and tunable without causing permanent changes in the genome, it may hold certain advantages in therapeutic applications. For RNA editing of adenosines, members of adenosine deaminase acting on the RNA (ADAR) family, such as ADAR1 (isoforms p110 and p150) and ADAR2 (refs. [2,3]), have been engineered for the precise conversion of adenosine (A) to inosine (I)[1]. The catalytic substrate of ADAR1/2 is double-stranded RNA, and the deaminase domain of ADAR1/2 is responsible for A-to-I RNA editing[4,5]. Inosine is recognized as guanosine (G) and paired with cytidine (C) in subsequent cellular translation processes[3]. To achieve targeted RNA editing, the ADAR protein—or its deaminase domain $ADAR_{DD}$—has been fused to a variety of RNA-targeting modules, such as a λN-peptide[6–8], a SNAP-tag[9–13] and a Cas13 protein[14]. In addition, targeted RNA editing can be achieved with engineered guide RNAs bearing an R/G motif coupled with ectopically expressed ADAR1 or ADAR2 proteins[15–18].

However, ectopic expression of exogenous editing enzymes is associated with several concerns, including substantial global off-target editing of the genome and/or RNA transcripts[19–23], immunogenicity[24–27], oncogenicity[28–30] and delivery hurdles[24]. Two RNA editing technologies, RESTORE[31] and LEAPER[32], reported by the Stafforst group and our own, leverage endogenous ADARs for programmable editing of RNA without the need to introduce exogenous proteins. LEAPER uses an engineered linear arRNA that can be generated through either expression in vivo via viral vectors or chemical synthesis in vitro. To enhance the capabilities of this system, here we aimed to enhance its editing efficiency and minimize its off-target edits. Because editing efficiency depends on the abundance and stability of arRNAs, we evaluated the use of circular RNA, a large class of noncoding RNAs that is highly stable because its covalently closed ring structure protects it from exonucleases[33–35].

Results

Pol II promoter-driven arRNAs enable efficient RNA editing. We first tested the ability of the Pol II promoter to drive arRNA transcription rather than U6, the weaker Pol III promoter we previously employed[32] (Supplementary Fig. 1a). Using a surrogate reporter based on mCherry and enhanced green fluorescent protein (eGFP) fluorescence[32], we found that the CMV promoter enabled a much higher level of arRNA expression than U6 (Supplementary Fig. 1b). Consistently, RNA editing efficiency was indeed significantly higher when the CMV promoter was used than when the U6 promoter was used (Supplementary Fig. 1c). These results suggest that arRNA abundance is critical for LEAPER efficiency and that the 5′ cap and 3′ poly(A) tail do not interfere with arRNAs in targeted RNA editing.

Circular arRNAs enable efficient and long-lasting programmable RNA editing. We assessed the effect of circularization of arRNAs, because circular RNA tends to have better stability and a longer half-life than linear RNA[33–37]. We generated circular arRNAs, termed circ-arRNAs, using a genetically encoded approach based on a previous report[36] (Fig. 1a). Sanger sequencing results indicated

[1]Biomedical Pioneering Innovation Center, Beijing Advanced Innovation Center for Genomics, Peking-Tsinghua Center for Life Sciences, Peking University Genome Editing Research Center, State Key Laboratory of Protein and Plant Gene Research, School of Life Sciences, Peking University, Beijing, China. [2]Academy for Advanced Interdisciplinary Studies, Peking University, Beijing, China. [3]EdiGene Inc., Life Science Park, Changping District, Beijing, China. [4]These authors contributed equally: Zongyi Yi, Liang Qu, Huixian Tang. ✉e-mail: wswei@pku.edu.cn

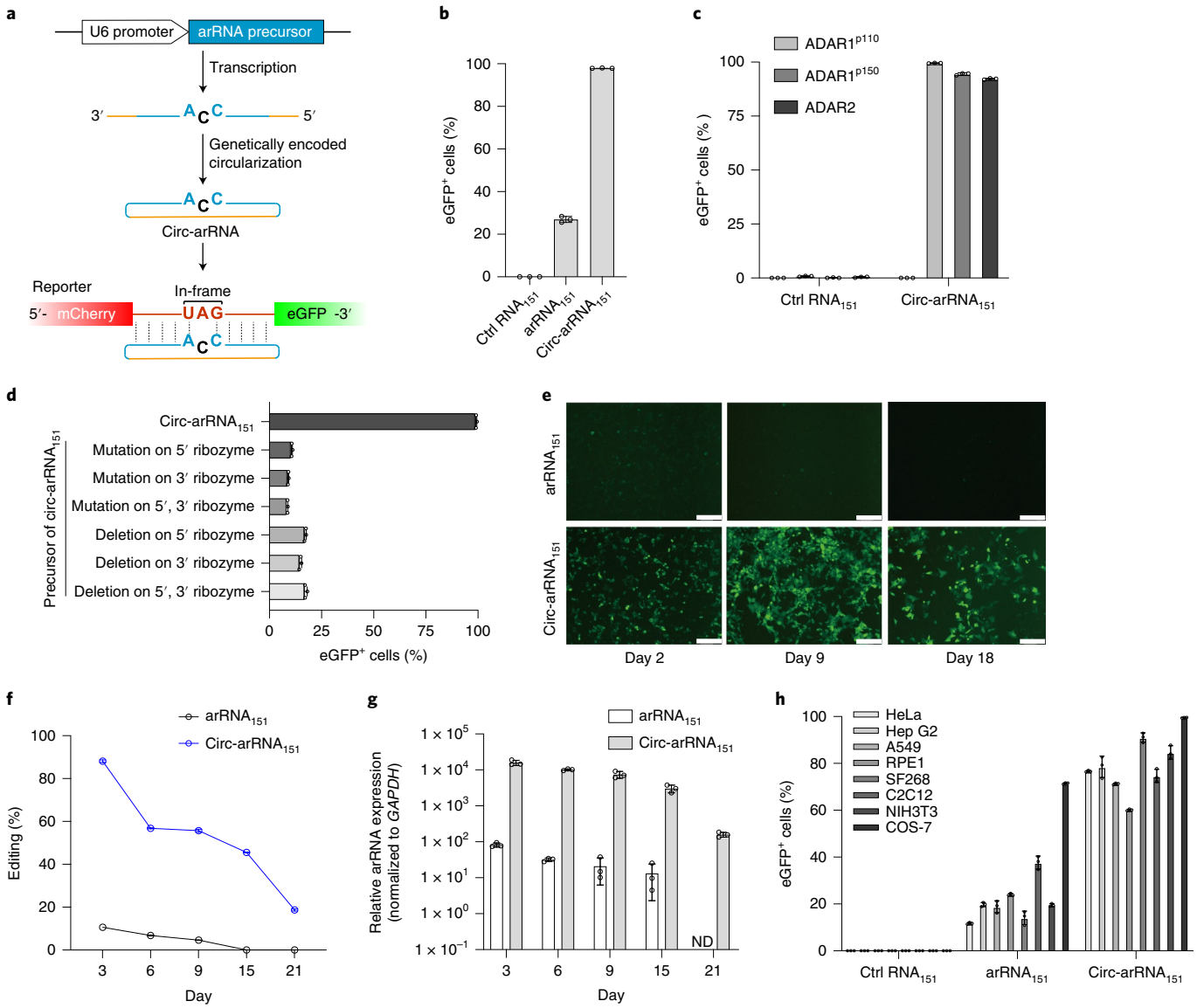

Fig. 1 | Leveraging endogenous ADAR for programmable RNA editing by genetically encoded circ-arRNAs. a, Schematic of genetically encoded circ-arRNAs. **b**, eGFP$^+$ percentages showing the editing efficiency of different arRNA versions targeting reporter transcripts in HEK293T cells with stable reporter expression; $n=3$, mean ± s.d. **c**, eGFP expression ratios induced by expression of *ADAR1*^{p110}, *ADAR1*^{p150} or *ADAR2* cDNA in *ADAR1* knockout (HEK293T *ADAR1*$^{-/-}$) cells; $n=3$, mean ± s.d. **d**, eGFP$^+$ percentage showing the effects of variable precursor RNA editing efficiency. Elements of circ-arRNA precursor were mutated or deleted in the 5′ P3 Twister U2A ribozyme and/or 3′ P1 Twister ribozyme that flank the ligation and arRNA sequences; $n=3$, mean ± s.d. **e**, Observation of eGFP expression in HEK293T cells with stable reporter expression after transfection with U6-driven linear arRNAs and circ-arRNAs on days 2, 9 and 18. Scale bars, 200 μm. **f**, Targeted transcript editing rates at different time points after transfection by arRNAs targeting reporter; $n=2$, mean ± s.d. **g**, Relative expression level of arRNAs at different time points after transfection by arRNAs targeting reporter, normalized to *GAPDH*; $n=3$, mean ± s.d; ND, no detection. **h**, eGFP$^+$ percentages showing the editing efficiency of different versions of arRNA-targeting reporter transcripts in multiple cell lines; $n=3$, mean ± s.d. **b**–**d**,**h**, eGFP$^+$ percentages were normalized by transfection efficiency, which was determined by mCherry$^+$.

that circ-arRNAs had been successfully produced (Supplementary Fig. 2a,b). Again, the CMV promoter produced greater amounts of linear arRNAs than U6 (Supplementary Fig. 2c). The abundance of circ-arRNAs was much higher than that of CMV promoter-driven arRNAs, even under the control of the U6 promoter (Supplementary Fig. 2c). We wondered whether we could further increase RNA production by combining the Pol II promoter and the RNA circularization strategy. However, U6 promoter-driven circ-arRNAs outperformed CMV promoter-driven circ-arRNAs in targeted RNA editing, as indicated by eGFP expression in a surrogate reporter assay[32] (Supplementary Fig. 2d), although the editing efficiency for both was significantly higher than their linear counterparts. We reason that the 5′ cap and 3′ poly(A) tail contribute significantly to the stability of RNAs, but that both modifications are nonfunctional because they are removed after arRNA circularization and the CMV promoter is weaker than U6 in expressing circ-arRNAs (Supplementary Fig. 2e). In addition, it is very likely that the 5′ cap and 3′ poly(A) tail interfere with the arRNA circularization process. Therefore, we decided to use the Pol III promoter to produce the circular version of arRNA.

The circ-arRNAs exhibited greater editing efficiency than linear arRNAs, as manifested by the significantly increased eGFP$^+$ percentages among transfected cells (Fig. 1b and Supplementary Fig. 1d). Such targeted RNA editing by the circular version of

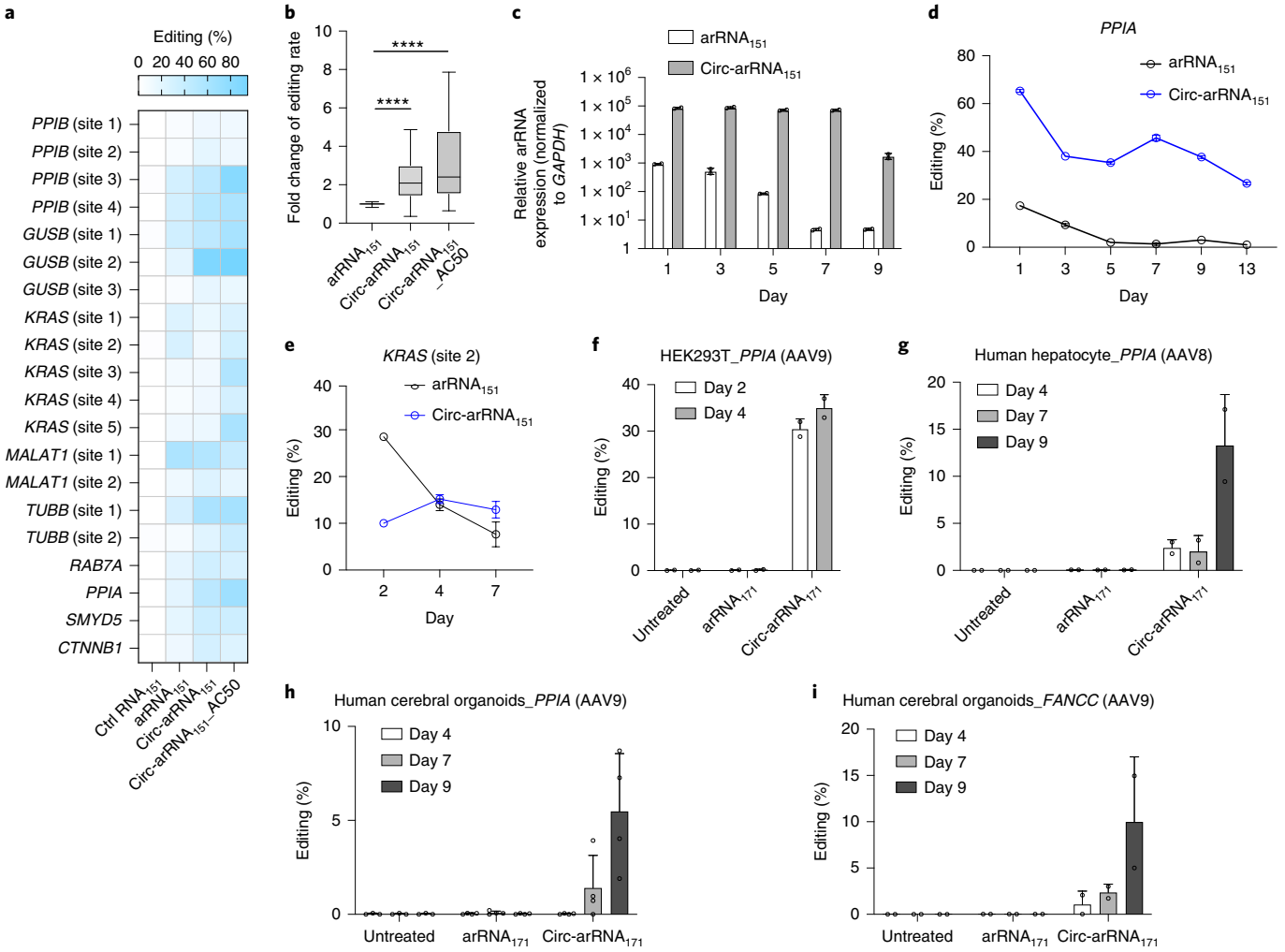

Fig. 2 | Circ-arRNAs enable efficient and long-lasting programmable RNA editing on endogenous transcripts. a, NGS results showing the rate of targeted adenosine editing in transcripts *PPIB*, *GUSB*, *KRAS*, *MALAT1*, *TUBB*, *RAB7A*, *PPIA*, *SMYD5* and *CTNNB1* by U6-driven linear arRNA$_{151}$, circ-arRNA$_{151}$ and circ-arRNA$_{151}$_AC50 in HEK293T cells; $n=3$. **b**, Respective fold change of editing rate normalized to linear arRNAs. Significance was analyzed using a two-tailed unpaired Student's *t*-test; ****$P=1.33124\times10^{-10}$ for circ-arRNA$_{151}$ and $P=1.20289\times10^{-10}$ for circ-arRNA$_{151}$_AC50; center line, medians; limits, 75% and 25%; whiskers, maximum and minimum; $n=3$ per site, 20 sites. **c**, Relative expression level of circ-arRNAs targeting *PPIA*, normalized to *GAPDH*; $n=2$, mean ± s.d. **d**,**e**, Long-lasting editing of cric-arRNAs of the endogenous site (*PPIA* (**d**), *KRAS* site 2 (**e**)) shows targeted transcript editing rates at different time points after transfection; $n=2$, mean ± s.d.. **f**–**i**, NGS results showing rates of targeted editing in HEK293T cells (**f**), human primary hepatocytes (**g**) and cerebral organoids (*PPIA* (**h**) and *FANCC* (**i**)) infected by AAV-delivered circ-arRNAs; **f**–**h**, $n=2$; **i**, $n=4$; mean ± s.d.

arRNAs was also mediated by endogenous ADAR1 proteins, because the editing-generated eGFP signal completely disappeared in HEK293T ADAR$^{-/-}$ cells but was rescued by three types of ADAR protein (Fig. 1c). To further confirm whether enhanced RNA editing was due to circularization of arRNAs, we created different types of mutation or deletion on ribozymes required for the formation of circ-arRNAs. Either point mutation or deletion in the ribozyme region of the circ-arRNA precursor significantly reduced the eGFP^{+} ratio to a level equivalent to that of linear arRNAs (Fig. 1d), indicating that it is circularization of arRNAs that enables elevated efficiency on targeted RNA editing. Moreover, circ-arRNA-mediated RNA editing was much more persistent, lasting up to 21 days (Fig. 1e,f and Supplementary Fig. 3), possibly due to the inherent stability of circ-arRNAs (Fig. 1g). RNA editing efficiency reached 90% of peak activity on day 3 post transfection, and remained high until the day 21 when tested (Fig. 1f). Similar to arRNAs, circ-arRNAs were detected in both the nucleus and cytoplasm, indicating that they may mediate targeted RNA editing both within and outside the nucleus (Supplementary Fig. 4a,b). Apart from HEK293T cells, we further demonstrated that circ-arRNAs also outperformed their linear counterparts in a panel of cell types, including HeLa, Hep G2, A549, RPE1, SF268, C2C12, NIH3T3 and COS-7 (Fig. 1h), indicating that circularization of arRNAs is a versatile strategy in achieving efficient and long-lasting targeted RNA editing.

Next, we explored whether circ-arRNAs could also enable efficient targeted RNA editing of endogenous transcripts. We designed 151-nt circ-arRNAs to target 20 different RNA sites of nine endogenous genes, *PPIB*, *GUSB*, *KRAS*, *MALAT1*, *TUBB*, *RAB7A*, *PPIA*, *SMYD5* and *CTNNB1* (Fig. 2a and Supplementary Table 1). Next-generation sequencing (NGS) analysis revealed that circ-arRNAs outperformed their linear counterparts in targeted RNA editing at 17 of 20 sites. However, circ-arRNAs showed a comparable editing rate on *MALAT1* (site 1) and even a decreased editing rate on *KRAS* (sites 1 and 2) (Fig. 2a). We speculated that circ-arRNAs targeting these three sites might have certain structures that interfered with their target recognition or functions to

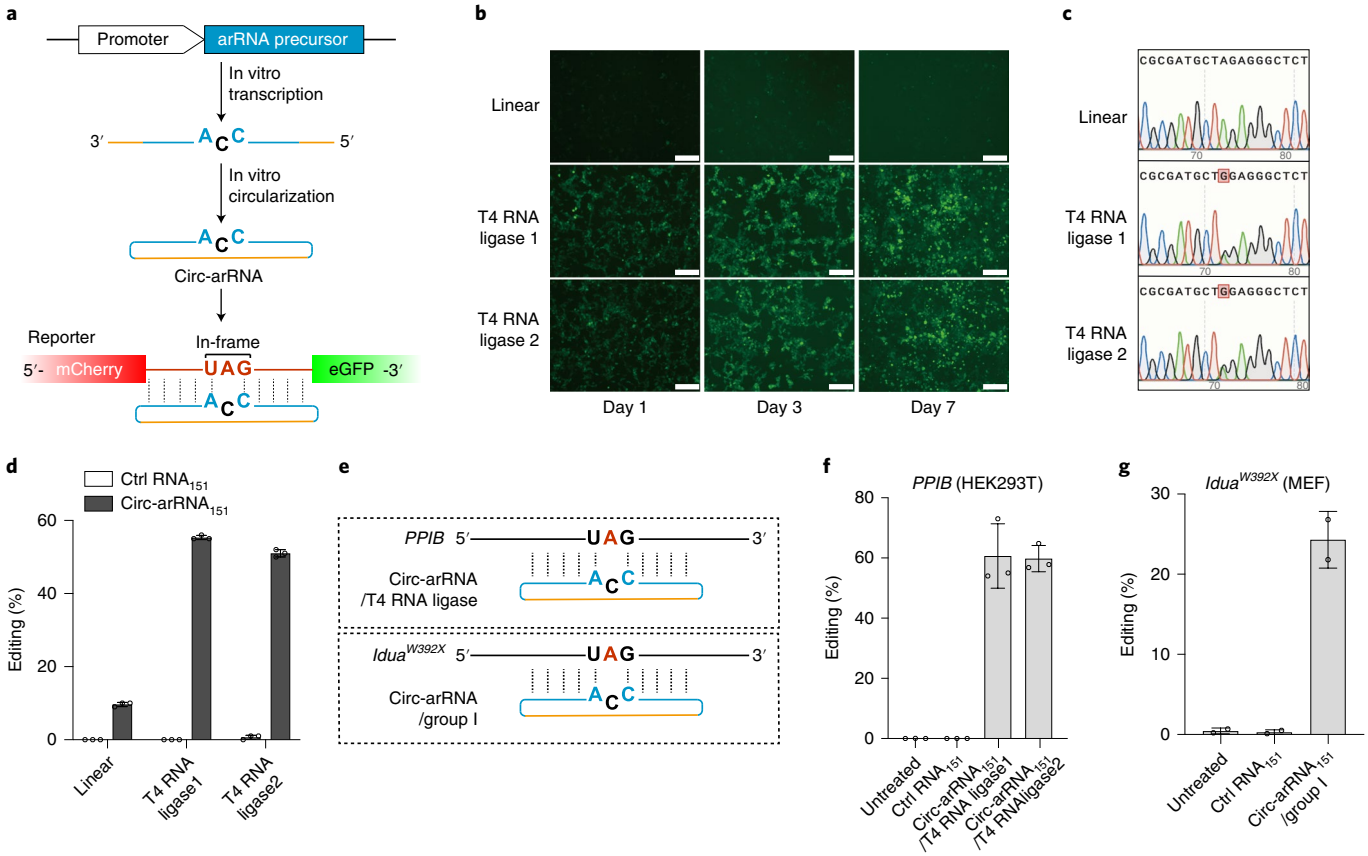

Fig. 3 | Leveraging endogenous ADAR protein for programmable RNA editing with in vitro-transcribed circ-arRNAs. a, Schematic of in vitro-produced circ-arRNAs. **b**, Observation of eGFP expression in HEK293T cells stably expressing reporter after transfection with linear precursor and purified circ-arRNAs cyclized by T4 RNA ligase on days 1, 3 and 7. Scale bars, 200 μm. **c**, Electropherograms showing Sanger sequencing results of the targeted region after transfection with precursor (top), T4 RNA ligase 1-ligated circ-arRNAs (middle) and T4 RNA ligase 2-ligated circ-arRNAs (bottom). **d**, NGS analysis of editing rates at the targeted site in reporter transcripts; $n = 3$, mean ± s.d. **e**, Schematic of the targeting of endogenous transcripts of *PPIB* and mouse *Idua* transcripts and corresponding circ-arRNAs. **f**, NGS results showing rates of targeted adenosine editing in *PPIB* transcripts upon introduction of T4 RNA ligase-cyclized circ-arRNAs into HEK293T cells; $n = 3$, mean ± s.d. **g**, NGS results showing rates of targeted adenosine editing in *Idua* transcripts upon introduction of group I ribozyme autocatalysis-ligated circ-arRNAs into primary MEFs generated from Hurler syndrome mice; $n = 2$, mean ± s.d.

mediate targeted editing activity. We thus tested whether the addition of flexible RNA linkers flanking circ-arRNAs could further optimize their ability in mediating editing activity. Fifty-nucleotide flexible polyAC RNA linkers, termed AC50, were added to flanking circ-arRNA$_{151}$, and these circ-arRNA_AC50 linkers gave rise to improved editing rates at 14 sites compared with circ-arRNA$_{151}$ (Fig. 2a). The circ-arRNA_AC50 targeting *KRAS* (sites 1 and 2) did elevate the editing efficiency of the original circ-arRNAs to a level comparable to that of corresponding linear arRNAs. On average, the editing efficiency of circ-arRNA and circ-arRNA_AC50 was 2.3- and 3.1-fold higher than their linear counterparts, respectively (Fig. 2b).

Because circ-arRNAs are more stable than their linear counterparts, we investigated RNA editing at two sites, *PPIA* and *KRAS* (site 2), over periods of up to 13 and 7 days, respectively. For *PPIA*, the expression level of circ-arRNAs was higher than for their corresponding linear counterparts (Fig. 2c). Consistent with the expression level of arRNAs, editing lasted for only 5 and >13 days for linear arRNAs and circ-arRNAs, respectively (Fig. 2d). For *KRAS* (site 2), although editing efficiency of linear arRNAs was higher than circ-arRNAs at the beginning (day 2), the editing rate of circ-arRNAs quickly surpassed that of their linear counterparts (days 4 and 7) because of the much faster degradation of the latter (Fig. 2e).

We also used adeno-associated virus (AAV) to deliver circ-arRNAs into HEK293T cells, human primary hepatocytes and human cerebral organoids. NGS results showed that AAV-delivered circ-arRNAs yielded much higher levels of targeted editing in all these cells and organoids than their linear counterparts, and in a long-lasting fashion (Fig. 2f–i).

Utilization of in vitro circularization strategies to generate circ-arRNAs. In addition to the genetically encoded circularization strategy, we tested an in vitro strategy to generate circ-arRNAs (Fig. 3a). Linear arRNAs from in vitro transcription were cyclized by T4 RNA ligase[38] and purified using high-performance liquid chromatography (HPLC) (Supplementary Fig. 5a). Ribonuclease H (RNaseH) cleavage assay further confirmed the purifity of in vitro-cyclized circ-arRNAs (Supplementary Fig. 5b). After transfection into HEK293T cells harboring the eGFP reporter (Fig. 3a)[32], purified circ-arRNAs generated much stronger and longer-lasting eGFP signals than their linear precursors (Fig. 3b). Targeted RNA editing rates for circ-arRNAs were more than fivefold higher than for linear precursors, as revealed by both Sanger sequencing (Fig. 3c) and NGS analysis (Fig. 3d). Moreover, in vitro-transcribed circ-arRNAs achieved an editing rate of >50% for endogenous *PPIB* transcripts (Fig. 3e,f). In a separate test of in vitro circularization,

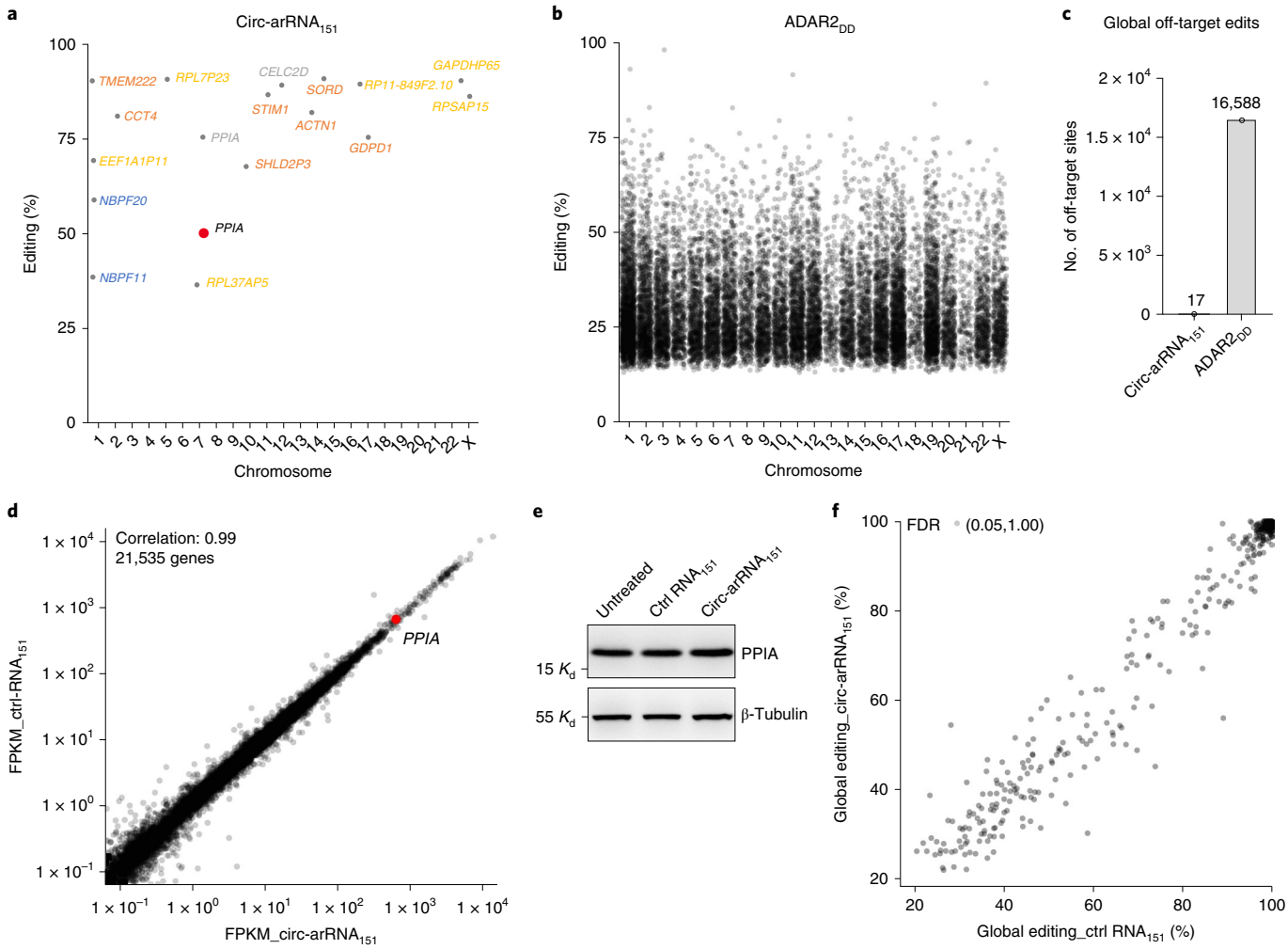

Fig. 4 | Transcriptome-wide specificity of RNA editing by circ-arRNAs. a,**b**, Analysis of transcriptome-wide off-target editing in the circ-arRNA$_{151}$ group (**a**) and ADAR2$_{DD}$ overexpression group (**b**). The on-targeting site (*PPIA*) is highlighted in red, and potential off-target sites identified in the *PPIA*-targeting RNA and ADAR2$_{DD}$ overexpression groups in gray. Annotation of off-target sites is shown in **a**. **c**, Numbers of transcriptome-wide off-target sites in the circ-arRNA$_{151}$ and ADAR2$_{DD}$ overexpression groups. **d**, Differential gene expression analysis of the effects of Ctrl RNA$_{151}$ and circ-arRNA$_{151}$ from RNA-seq data at the transcriptome level. FPKM value was calculated with the STRINGTIE tool, and Pearson's correlation coefficient analysis was used to assess global differential gene expression. **e**, Immunoblot showing PPIA protein expression level in cells transfected by Ctrl RNA$_{151}$ and circ-arRNA$_{151}$-*PPIA*. **f**, Transcriptome-wide analysis of the effects of circ-arRNA$_{151}$-*PPIA* on 1,498 native editing sites. FDR, false discovery rate.

we investigated the use of group I ribozyme-mediated autocatalysis[37,39] to generate circ-arRNAs (Fig. 3e). NGS results showed that the circ-arRNAs generated by group I ribozyme autocatalysis were able to correct the pathogenic point mutations of *IDUA*^{W392X} transcripts in mouse embryonic fibroblasts (MEFs) derived from a mouse model of Hurler syndrome, with an editing rate of approximately 25% (Fig. 3g). Collectively, these data demonstrate that circ-arRNAs either generated by genetically encoded strategy or produced in vitro can achieve efficient and long-lasting targeted RNA editing in endogenous transcripts.

RNA editing specificity of circ-arRNAs. We performed transcriptome-wide RNA sequencing analysis to evaluate the editing specificity of circ-arRNAs. HEK293T cells transfected with circ-arRNA$_{151}$-*PPIA*-expressing plasmids were subjected to transcriptome-wide RNA sequencing (RNA-seq) analysis, in which nontargeting circular Ctrl RNA$_{151}$ was used as a control. We also tested an ADAR2 deaminase domain (ADAR2$_{DD}$)-overexpressing group, because overexpression of ADAR2$_{DD}$ has been used in many previously reported RNA editing tools[6–14]. Transcriptome-wide RNA-seq results showed there were 17 potential off-target edits in the circ-arRNA$_{151}$-*PPIA* transfection group (Fig. 4a). However, the ADAR2$_{DD}$ overexpression group resulted in nearly 16,588 off-target edits in the RNA transcriptome compared with the control (Fig. 4b), much higher than for circ-arRNA (Fig. 4c). Most of the 17 identified off-target sites in the circ-arRNA$_{151}$-*PPIA* transfection group were located in the intron and pseudogene regions (Supplementary Fig. 6a). Minimum free energy analysis indicated that all these off-target hits failed to form a stable duplex with circ-arRNA$_{151}$-*PPIA* (Supplementary Fig. 6b), and thus are unlikely to be actual sequence-dependent off-targets.

To test whether circ-arRNA$_{151}$-*PPIA* would affect the expression level of targeted *PPIA* transcripts, we used the above transcriptome-wide RNA-seq data for further analysis. Circ-arRNA$_{151}$-*PPIA*-mediated editing in *PPIA* transcripts affected neither the expression nor splicing pattern of *PPIA* transcripts (Fig. 4d and Supplementary Fig. 7a–c) and, consistent with our previous observations[32], neither was the protein level of PPIA affected (Fig. 4e). In addition, A-to-I RNA editing sites shared in the circ-arRNA$_{151}$-*PPIA* and control (Ctrl) RNA$_{151}$ groups were highly

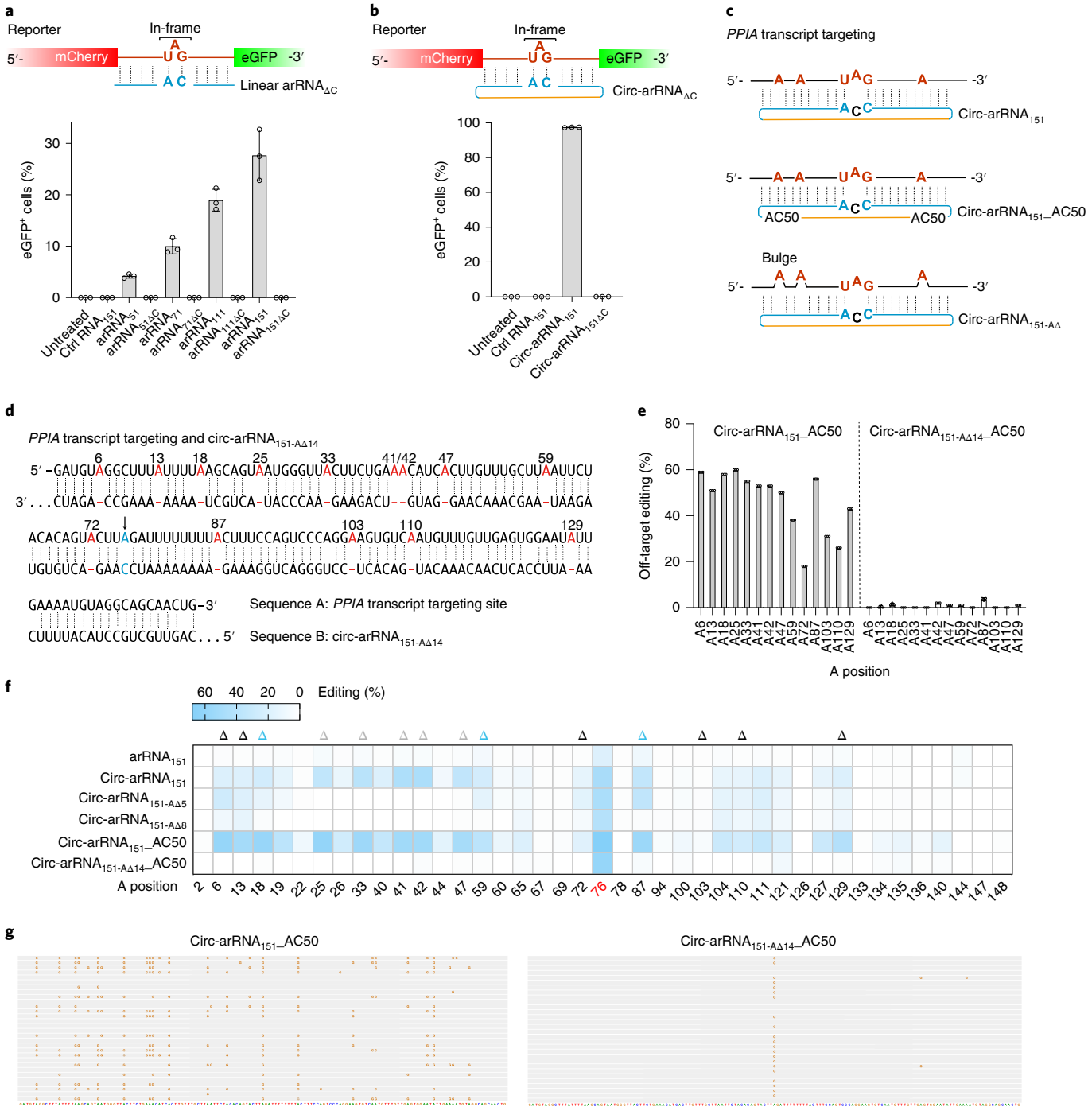

Fig. 5 | Engineered circ-arRNAs reduce bystander off-target editing. a, Percentages of eGFP$^+$ showing the efficiency of reporter transcript editing by arRNA and arRNA$_{\Delta C}$ in HEK293T cells with stable reporter expression; $n = 3$, mean ± s.d. **b**, Percentages of eGFP$^+$ showing the efficiency of reporter transcript editing by circ-arRNA and circ-arRNA$_{\Delta C}$ in HEK293T cells with stable reporter expression; $n = 3$, mean ± s.d. **c**, Schematic of the *PPIA* transcript sequence targeted by circ-arRNA$_{151}$ (top), circ-arRNA$_{151}$_AC50 (middle) and circ-arRNA$_{151\text{-}A\Delta}$ (bottom). **d**, Schematic of *PPIA* transcript sequence covered by 151-nt arRNA. Black arrow indicates the targeted adenosine, and potential off-target adenosines are marked in red. Circ-arRNA$_{151\text{-}A\Delta14}$ targeting *PPIA* transcripts with U deletion opposite A^{6th}, A^{13th}, A^{18th}, A^{25th}, A^{33rd}, A^{41st}, A^{42nd}, A^{47th}, A^{59th}, A^{72nd}, A^{87th}, A^{103rd}, A^{110th} and A^{129th} to minimize potential off-target edits in editing-prone motifs. **e**, Editing rates of off-target adenosines in circ-arRNA$_{151}$_AC50 and circ-arRNA$_{151\text{-}A\Delta14}$_AC50 groups; $n = 3$, mean ± s.d. **f**, Heatmap of editing rate for adenosines covered by circ-arRNA$_{151}$_AC50 and circ-arRNA$_{151\text{-}A\Delta14}$_AC50 in *PPIA* transcripts; $n = 3$. Gray triangles represent positions of U deletions in circ-arRNA$_{151\text{-}A\Delta5}$, blue triangles represent positions of additional U deletions in circ-arRNA$_{151\text{-}A\Delta8}$ based on circ-arRNA$_{151\text{-}A\Delta5}$. Positions of U deletions in circ-arRNA$_{151\text{-}A\Delta14}$_AC50 denoted by gray, blue and black triangles. **g**, IGV results showing editing reads in circRNA$_{151}$_AC50 and circ-arRNA$_{151\text{-}A\Delta14}$_AC50.

parallel to each other, indicating that circ-arRNAs have little impact on the normal A-to-I editing function of endogenous ADAR proteins (Fig. 4f).

Engineered circ-arRNAs reduce bystander off-target editing. In addition to transcriptome-wide off-target analysis, we tested bystander off-target edits on the arRNA-covered regions of the

targeted transcripts. Our previous results showed that A-G mismatching can significantly reduce the bystander off-target edits of arRNAs[32] because adenosine deamination requires an ADAR to flip the reactive base out of the RNA double helix to access its active site[40]. Based on the catalytic feature of ADAR1/2 (refs. [41–43]), we found that targeted RNA editing was completely eliminated when we deleted the nucleotide opposite the targeted adenosine in linear arRNAs (Fig. 5a) or circ-arRNAs (Fig. 5b). Based on this finding, we tested the use of such an approach to reduce bystander off-target edits by deleting nucleotides opposite to unwanted adenosines in circ-arRNA-covered regions (Fig. 5c). We designed different versions of circ-arRNAs targeting endogenous *PPIA* transcripts, circ-arRNA$_{151}$, circ-arRNA$_{151\text{-}A\Delta5}$, circ-arRNA$_{151\text{-}A\Delta8}$, circ-arRNA$_{151}$_AC50 and circ-arRNA$_{151\text{-}A\Delta14}$_AC50, in which we retained or deleted uridines on circ-arRNA opposite potential off-target sites (Fig. 5c,d and Supplementary Table 1). It is not uncommon in mammalian cells for adenosines in imperfect dsRNA with mismatches or bulges to be effectively edited by ADARs with high specificity and efficiency[44,45]. Notably, we found that circ-arRNA$_{151\text{-}A\Delta8}$ remarkably reduced off-target editing at all eight sites tested, and circ-arRNA$_{151\text{-}A\Delta14}$_AC50 almost eliminated all bystander off-targets while still maintaining 60% editing efficiency on the targeted site (Fig. 5e,f). NGS reads surrounding the on-target site showed that circ-arRNA$_{151\text{-}A\Delta14}$_AC50 could generate targeted editing with no bystander off-targets in >90% of edited transcripts (Fig. 5g).

We then tested in vitro-synthesized circ-arRNA$_{151\text{-}A\Delta14}$ and found that it could also achieve efficient editing in a dose-dependent manner (Supplementary Fig. 8). Consistent with our previous observation[32], circ-arRNAs with or without deletion did not affect the expression level of ADAR, nor elicit an innate immune response (Supplementary Fig. 9a,b).

Activation of Wnt signaling pathway via circ-arRNAs. To further confirm whether circ-arRNA-mediated targeted editing would affect protein function, we designed circ-arRNAs targeting the T41 codon of *CTNNB1* (ref. [46]) that converts threonine to alanine, to accumulate β-catenin and consequently to activate the Wnt pathway[46] (Fig. 6a). We found that circ-arRNA$_{151}$ yielded 32% editing at this site (Fig. 6b), leading to a 53-fold increase in activity of the β-catenin signal pathway while linear arRNA$_{151}$ generated an increase of only twofold (Fig. 6c).

Recovery of p53 transcriptional activity by circ-arRNAs with high efficiency and specificity. We explored potential therapeutic uses of circ-arRNAs aiming to target the *TP53* tumor suppressor gene, which undergoes frequent mutations in >50% of human cancers[47]. The c.158G-to-A variant of *TP53* is a clinically relevant non-sense mutation (Trp53Ter) generating a functional truncated protein (Fig. 6d). We designed different versions of circ-arRNAs targeting *TP53*^{W53X} flanked by flexible RNA linkers or harboring a U deletion (Fig. 6d,e). NGS analysis showed variable editing rates on the targeted adenosine: ~30% was achieved with circ-arRNA$_{151}$ while ~40% was achieved with circ-arRNA$_{151\text{-}AG1}$, circ-arRNA$_{151\text{-}AG4}$ and circ-arRNA$_{151\text{-}A\Delta1}$, with A-G mismatch or U deletion at one undesirable off-target site (Fig. 6f and Supplementary Table 1). All rates were higher with circ-arRNAs than with the corresponding linear arRNAs[32]. The circ-arRNA$_{151\text{-}A\Delta4}$ with a U deletion at four potential off-target site groups conferred an increased editing rate of ~50% (Fig. 6f).

We inserted 50-nt polyAC RNA linkers flanking the arRNA sequences in both circ-arRNA$_{151}$ and circ-arRNA$_{151\text{-}A\Delta4}$ (Fig. 6e). NGS analysis showed that such optimization with flexible linkers indeed increased targeted RNA editing efficiency at this site, especially for circ-arRNA$_{151\text{-}A\Delta4}$_AC50, which yielded ~70% of editing (Fig. 6f).

In addition to transcript editing, all versions of circ-arRNAs effectively rescued the production of full-length p53 protein in HEK293T *TP53*$^{-/-}$ cells (Supplementary Fig. 10a). Using a previously reported p53-luciferase *cis*-reporting system[48,49], we demonstrated that all versions of circ-arRNAs were able to restore the transcriptional regulation function of p53 (Fig. 6g). The circ-arRNA$_{151\text{-}A\Delta4}$_AC50, which exhibited the highest editing rate, restored transcriptional regulation activity to the greatest extent and was remarkably more effective than the linear arRNA version[32] (Fig. 6g).

Finally, we examined potential off-target edits in circ-arRNA-covered regions. As expected, deletion of the U nucleotide opposite the potential off-target A nucleotide on circ-arRNAs almost completely abolished bystander off-target edits at four predicted sites (Fig. 6h and Supplementary Fig. 10b), while it further increased the on-target editing rate (Fig. 6f). Of note, although circ-arRNA$_{151}$_AC50 showed higher editing efficiency than circ-arRNA$_{151\text{-}A\Delta4}$ at the targeted site (Fig. 6f), the functional recovery level of circ-arRNA$_{151\text{-}A\Delta4}$ was much higher than that of circ-arRNA$_{151}$_AC50 because of its low rate of bystander off-target effects (Fig. 6h and Supplementary Fig. 10b). Collectively, these results show that LEAPER 2.0 can significantly increase the on-target editing rate while eliminating off-target effects.

Restoration of α-L-iduronidase activity in Hurler syndrome mice by circ-arRNAs. Hurler syndrome is the most severe subtype of mucopolysaccharidosis type I, because of the deficiency of α-L-iduronidase (IDUA), a lysosomal metabolic enzyme responsible for the metabolism of mucopolysaccharides. We studied treatment of a mouse model of Hurler syndrome harboring a homozygous W392X (TGG-to-TAG) point mutation in exon 9 of *Idua*, which is analogous to the W402X mutation found in patients with Hurler syndrome[50]. We designed two versions of circ-arRNAs targeting the mature messenger RNA or pre-mRNA of *Idua* (Fig. 6i and Supplementary Table 1). Circ-arRNA$_{151}$/mRNA or circ-arRNA$_{151}$/pre-mRNA targeting was delivered to Idua-W392X

Fig. 6 | Activation and restoration of protein function in cell culture and Hurler syndrome mice by circ-arRNAs. a, Schematic of cells accumulating β-catenin and activating the Wnt signaling pathway. **b**, NGS analysis of editing rates at the targeted site in *CTNNB1* transcripts; $n = 3$, mean ± s.d. **c**, Activation fold change of Wnt signaling pathway by linear arRNAs and circ-arRNAs; $n = 2$, mean ± s.d. **d**, Schematic of the *TP53*^{W53X} transcript sequence covered by the 151-nt arRNA containing a c.158G-to-A clinically relevant non-sense mutation (Trp53Ter). Black arrow indicates the targeted adenosine. The design of circ-arRNAs targeting *TP53*^{W53X} transcripts with a U deletion opposite A^{66th}, together with A^{36th}, A^{111th}, and A^{114th}, to minimize potential off-target edits in editing-prone motifs. **e**, Schematic of the *TP53* transcript sequence targeted by circ-arRNA$_{151}$_AC50 (top) and circ-arRNA$_{151\text{-}A\Delta4}$_AC50 (bottom). **f**, NGS results showing targeted editing of *TP53*^{W53X} transcripts by circ-arRNA$_{151}$, circ-arRNA$_{151\text{-}AG1}$, circ-arRNA$_{151\text{-}AG4}$, circ-arRNA$_{151\text{-}A\Delta1}$, circ-arRNA$_{151\text{-}A\Delta4}$, circ-arRNA$_{151}$_AC50 and circ-arRNA$_{151\text{-}A\Delta4}$_AC50; $n = 3$, mean ± s.d. **g**, Detection of transcriptional regulatory activity of restored p53 protein using a p53-firefly luciferase reporter system, normalized by a cotransfected Renilla luciferase vector; $n = 3$, mean ± s.d. **h**, Editing efficiency at four potential off-target sites showing a reduction in bystander off-target editing via U deletions on circ-arRNA$_{151}$; $n = 3$, mean ± s.d. **i**, Schematic of the *Idua*^{W392X} transcript sequence targeted by circ-arRNA$_{151}$/mRNA targeting and circ-arRNA$_{151}$/pre-mRNA targeting. **j**, NGS results showing editing rates for targeted adenosine of *Idua* transcripts in mouse hepatocytes; $n = 4$ for control group, $n = 6$ for treatment groups, mean ± s.d. **k**, Measurement of the catalytic activity of IDUA with a 4-methylumbelliferyl IDUA substrate in different groups; $n = 4$, mean ± s.d. **l**, Tissue GAG content in wild type (WT) mice, IDUA^{W392X} mice and treatment groups; $n = 6$, mean ± SD. **m**, Relative quantitation of *Idua* expression in different treatment groups (normalized to *GAPDH*); $n = 4$, mean ± s.d.

mice via transduction of a self-complementary AAV (scAAV). Four weeks later, the mice were sacrificed and liver tissues were collected for the measurement of targeted RNA editing and catalytic activity of IDUA. NGS analysis revealed that both circ-arRNA$_{151}$/mRNA and circ-arRNA$_{151}$/pre-mRNA targeting achieved a ~10% targeted editing rate (Fig. 6j). Consistent with the sequencing results, both circ-arRNAs significantly restored IDUA catalytic activity in the liver tissues of Idua-W392X mice (Fig. 6k) while liver glycosaminoglycan (GAG) content also decreased in the circ-arRNA group (Fig. 6l). The presence of circ-arRNAs did not affect the abundance

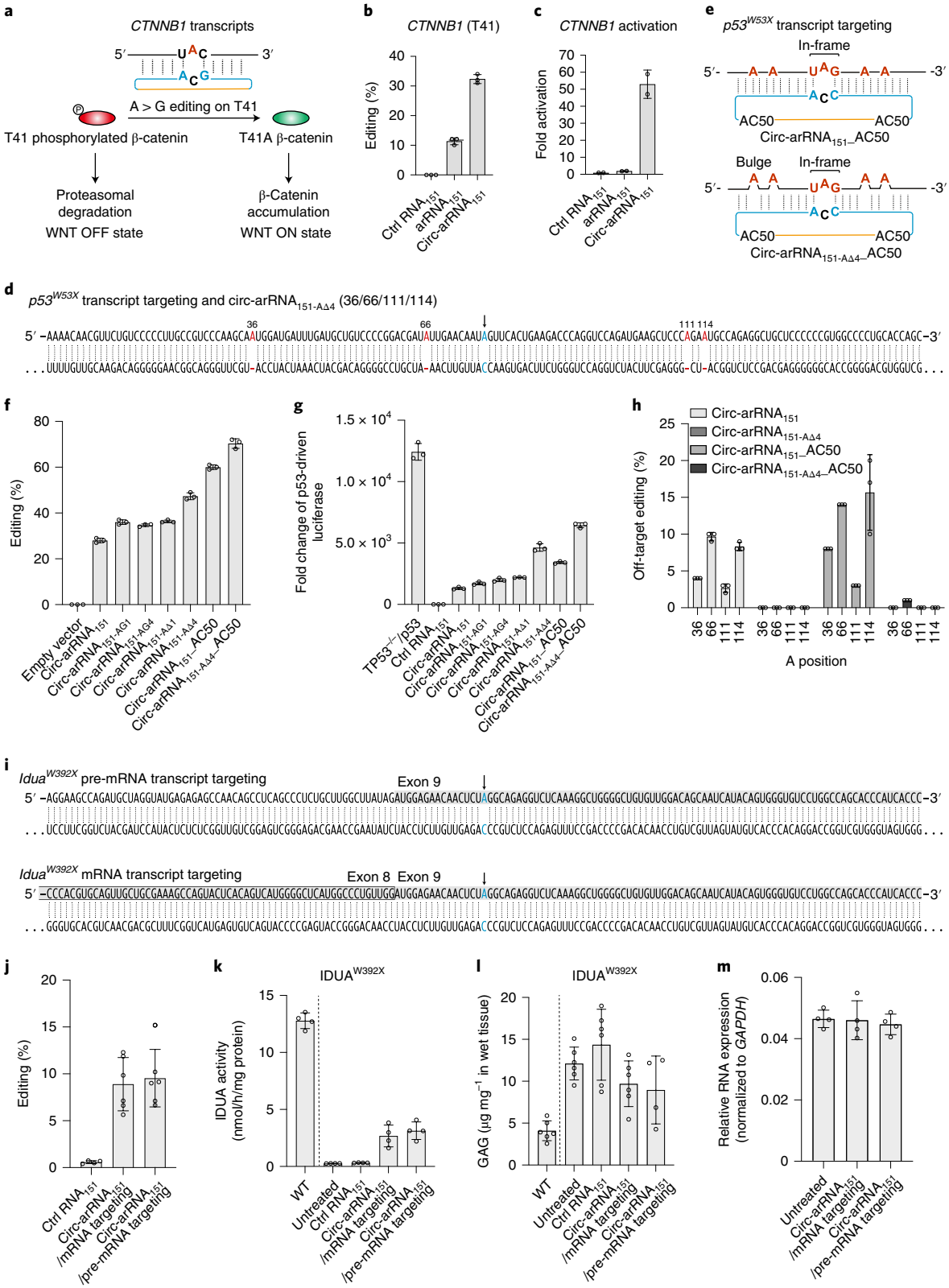

of *Idua* transcripts (Fig. 6m). These results demonstrate the potential of LEAPER 2.0 for precise, efficient and long-lasting targeted RNA editing in certain clinical genetic diseases.

Discussion

In this study, we improved our previously reported LEAPER system[32] by using engineered circ-arRNAs rather than linear arRNAs, achieving more efficient and specific targeted RNA editing of endogenous transcripts. Owing to their covalently closed ring structure, circ-arRNAs are more stable and resistant to degradation than linear arRNAs[33–35]. We demonstrate improved efficiency of targeted RNA editing, on average ~3.1-fold compared with linear arRNAs in most sites (Figs. 2a and 3d)[32]. Moreover, the time period of RNA editing is longer, up to 21 days (Fig. 1g), a potential benefit in therapeutic applications. Consistently, circ-arRNAs delivered through AAV or scAAV achieved long-lasting and much improved editing at the target site (Figs. 2 and 6).

Moreover, we engineered circ-arRNAs to reduce bystander off-target edits and improve the on-target editing rate. LEAPER 2.0 causes fewer transcriptome-wide off-target edits compared with ectopic expression of $ADAR2_{DD}$ (Fig. 4). The major off-target edits of LEAPER are bystander off-target edits within the targeted RNA region covered by arRNAs, and we previously reported an approach to minimization of such off-target edits using an A-G mismatch strategy[32]. We sought to further minimize such off-target edits with LEAPER 2.0, and found that additional engineering of circ-arRNAs with U deletion opposite potential off-target adenosines significantly reduced site-specific bystander off-target edits in the circ-arRNA-covered region (Figs. 5e–g and 6h). Moreover, the engineered circ-arRNAs improved the rate of on-target editing in $TP53^{W53X}$ transcripts (Fig. 6f). The introduction of flexible RNA linkers flanking arRNA further enhanced the on-targeting editing rate of circ-arRNA at most sites (Figs. 2a, 5f and 6f), and other types of linkers with similar effects remain to be explored.

Finally, we have demonstrated that circ-arRNAs can either be delivered as in vitro-transcribed RNA oligonucleotides (Fig. 3) or expressed in vivo using an AAV vector (Figs. 2 and 6). Circ-arRNAs delivered into Hurler syndrome model mice via scAAV transduction successfully corrected a pathogenic mutation of $Idua^{W392X}$ and restored IDUA catalytic activity. Circ-arRNAs are well suited for delivery by a variety of nonviral vehicles, including lipid nanoparticles[51] and clinical antisense oligonucleotide RNA drugs[52,53]. Collectively, LEAPER 2.0 enables precise, efficient RNA editing with broad applicability for therapy and basic research.

Online content

Any methods, additional references, Nature Research reporting summaries, source data, extended data, supplementary information, acknowledgements, peer review information; details of author contributions and competing interests; and statements of data and code availability are available at https://doi.org/10.1038/s41587-021-01180-3.

Received: 12 June 2021; Accepted: 1 December 2021;
Published online: 10 February 2022

References

1. Fry, L. E., Peddle, C. F., Barnard, A. R., McClements, M. E. & MacLaren, R. E. RNA editing as a therapeutic approach for retinal gene therapy requiring long coding sequences. *Int. J. Mol. Sci.* **21**, 277 (2020).
2. Tan, M. H. et al. Dynamic landscape and regulation of RNA editing in mammals. *Nature* **550**, 249–254 (2017).
3. Nishikura, K. Functions and regulation of RNA editing by ADAR deaminases. *Annu. Rev. Biochem.* **79**, 321–349 (2010).
4. Bass, B. L. & Weintraub, H. An unwinding activity that covalently modifies its double-stranded RNA substrate. *Cell* **55**, 1089–1098 (1988).
5. Wong, S. K., Sato, S. & Lazinski, D. W. Substrate recognition by ADAR1 and ADAR2. *RNA* **7**, 846–858 (2001).
6. Montiel-Gonzalez, M. F., Vallecillo-Viejo, I., Yudowski, G. A. & Rosenthal, J. J. Correction of mutations within the cystic fibrosis transmembrane conductance regulator by site-directed RNA editing. *Proc. Natl Acad. Sci. USA* **110**, 18285–18290 (2013).
7. Sinnamon, J. R. et al. Site-directed RNA repair of endogenous Mecp2 RNA in neurons. *Proc. Natl Acad. Sci. USA* **114**, E9395–E9402 (2017).
8. Montiel-Gonzalez, M. F., Vallecillo-Viejo, I. C. & Rosenthal, J. J. An efficient system for selectively altering genetic information within mRNAs. *Nucleic Acids Res.* **44**, e157 (2016).
9. Hanswillemenke, A., Kuzdere, T., Vogel, P., Jekely, G. & Stafforst, T. Site-directed RNA editing in vivo can be triggered by the light-driven assembly of an artificial riboprotein. *J. Am. Chem. Soc.* **137**, 15875–15881 (2015).
10. Schneider, M. F., Wettengel, J., Hoffmann, P. C. & Stafforst, T. Optimal guideRNAs for re-directing deaminase activity of hADAR1 and hADAR2 in trans. *Nucleic Acids Res.* **42**, e87 (2014).
11. Vogel, P., Hanswillemenke, A. & Stafforst, T. Switching protein localization by site-directed RNA editing under control of light. *ACS Synth. Biol.* **6**, 1642–1649 (2017).
12. Vogel, P., Schneider, M. F., Wettengel, J. & Stafforst, T. Improving site-directed RNA editing in vitro and in cell culture by chemical modification of the guideRNA. *Angew. Chem. Int. Ed. Engl.* **53**, 6267–6271 (2014).
13. Vogel, P. et al. Efficient and precise editing of endogenous transcripts with SNAP-tagged ADARs. *Nat. Methods* **15**, 535–538 (2018).
14. Cox, D. B. T. et al. RNA editing with CRISPR-Cas13. *Science* **358**, 1019–1027 (2017).
15. Fukuda, M. et al. Construction of a guide-RNA for site-directed RNA mutagenesis utilising intracellular A-to-I RNA editing. *Sci. Rep.* **7**, 41478 (2017).
16. Wettengel, J., Reautschnig, P., Geisler, S., Kahle, P. J. & Stafforst, T. Harnessing human ADAR2 for RNA repair – recoding a PINK1 mutation rescues mitophagy. *Nucleic Acids Res.* **45**, 2797–2808 (2017).
17. Heep, M., Mach, P., Reautschnig, P., Wettengel, J. & Stafforst, T. Applying human ADAR1p110 and ADAR1p150 for site-directed RNA editing-G/C substitution stabilizes guideRNAs against editing. *Genes (Basel)* **8**, 34 (2017).
18. Katrekar, D. et al. In vivo RNA editing of point mutations via RNA-guided adenosine deaminases. *Nat. Methods* **16**, 239–242 (2019).
19. Zhou, C. et al. Off-target RNA mutation induced by DNA base editing and its elimination by mutagenesis. *Nature* **571**, 275–278 (2019).
20. Grunewald, J. et al. Transcriptome-wide off-target RNA editing induced by CRISPR-guided DNA base editors. *Nature* **569**, 433–437 (2019).
21. Grunewald, J. et al. CRISPR DNA base editors with reduced RNA off-target and self-editing activities. *Nat. Biotechnol.* **37**, 1041–1048 (2019).
22. Jin, S. et al. Cytosine, but not adenine, base editors induce genome-wide off-target mutations in rice. *Science* **364**, 292–295 (2019).
23. Vallecillo-Viejo, I. C., Liscovitch-Brauer, N., Montiel-Gonzalez, M. F., Eisenberg, E. & Rosenthal, J. J. C. Abundant off-target edits from site-directed RNA editing can be reduced by nuclear localization of the editing enzyme. *RNA Biol.* **15**, 104–114 (2018).
24. Chew, W. L. et al. A multifunctional AAV-CRISPR-Cas9 and its host response. *Nat. Methods* **13**, 868–874 (2016).
25. Wagner, D. L. et al. High prevalence of *Streptococcus pyogenes* Cas9-reactive T cells within the adult human population. *Nat. Med.* **25**, 242–248 (2019).
26. Simhadri, V. L. et al. Prevalence of pre-existing antibodies to CRISPR-associated nuclease Cas9 in the USA population. *Mol. Ther. Methods Clin. Dev.* **10**, 105–112 (2018).
27. Charlesworth, C. T. et al. Identification of preexisting adaptive immunity to Cas9 proteins in humans. *Nat. Med.* **25**, 249–254 (2019).
28. Teoh, P. J. et al. Aberrant hyperediting of the myeloma transcriptome by ADAR1 confers oncogenicity and is a marker of poor prognosis. *Blood* **132**, 1304–1317 (2018).
29. Haapaniemi, E., Botla, S., Persson, J., Schmierer, B. & Taipale, J. CRISPR-Cas9 genome editing induces a p53-mediated DNA damage response. *Nat. Med.* **24**, 927–930 (2018).
30. Ihry, R. J. et al. p53 inhibits CRISPR-Cas9 engineering in human pluripotent stem cells. *Nat. Med.* **24**, 939–946 (2018).
31. Merkle, T. et al. Precise RNA editing by recruiting endogenous ADARs with antisense oligonucleotides. *Nat. Biotechnol.* **37**, 133–138 (2019).
32. Qu, L. et al. Programmable RNA editing by recruiting endogenous ADAR using engineered RNAs. *Nat. Biotechnol.* **37**, 1059–1069 (2019).
33. Memczak, S. et al. Circular RNAs are a large class of animal RNAs with regulatory potency. *Nature* **495**, 333–338 (2013).
34. Enuka, Y. et al. Circular RNAs are long-lived and display only minimal early alterations in response to a growth factor. *Nucleic Acids Res.* **44**, 1370–1383 (2016).
35. Kristensen, L. S. et al. The biogenesis, biology and characterization of circular RNAs. *Nat. Rev. Genet.* **20**, 675–691 (2019).
36. Litke, J. L. & Jaffrey, S. R. Highly efficient expression of circular RNA aptamers in cells using autocatalytic transcripts. *Nat. Biotechnol.* **37**, 667–675 (2019).

37. Wesselhoeft, R. A., Kowalski, P. S. & Anderson, D. G. Engineering circular RNA for potent and stable translation in eukaryotic cells. *Nat. Commun.* **9**, 2629 (2018).
38. Beaudry, D. & Perreault, J. P. An efficient strategy for the synthesis of circular RNA molecules. *Nucleic Acids Res.* **23**, 3064–3066 (1995).
39. Puttaraju, M. & Been, M. D. Group I permuted intron-exon (PIE) sequences self-splice to produce circular exons. *Nucleic Acids Res.* **20**, 5357–5364 (1992).
40. Kuttan, A. & Bass, B. L. Mechanistic insights into editing-site specificity of ADARs. *Proc. Natl Acad. Sci. USA* **109**, E3295–E3304 (2012).
41. Wahlstedt, H. & Ohman, M. Site-selective versus promiscuous A-to-I editing. *Wiley Interdiscip. Rev. RNA* **2**, 761–771 (2011).
42. Gallo, A., Vukic, D., Michalik, D., O'Connell, M. A. & Keegan, L. P. ADAR RNA editing in human disease; more to it than meets the I. *Hum. Genet.* **136**, 1265–1278 (2017).
43. Eggington, J. M., Greene, T. & Bass, B. L. Predicting sites of ADAR editing in double-stranded RNA. *Nat. Commun.* **2**, 319 (2011).
44. Bazak, L. et al. A-to-I RNA editing occurs at over a hundred million genomic sites, located in a majority of human genes. *Genome Res.* **24**, 365–376 (2014).
45. Tian, N. et al. A structural determinant required for RNA editing. *Nucleic Acids Res.* **39**, 5669–5681 (2011).
46. MacDonald, B. T., Tamai, K. & He, X. Wnt/beta-catenin signaling: components, mechanisms, and diseases. *Dev. Cell* **17**, 9–26 (2009).
47. Floquet, C., Deforges, J., Rousset, J. P. & Bidou, L. Rescue of non-sense mutated p53 tumor suppressor gene by aminoglycosides. *Nucleic Acids Res.* **39**, 3350–3362 (2011).
48. Kern, S. E. et al. Identification of p53 as a sequence-specific DNA-binding protein. *Science* **252**, 1708–1711 (1991).
49. Doubrovin, M. et al. Imaging transcriptional regulation of p53-dependent genes with positron emission tomography in vivo. *Proc. Natl Acad. Sci. USA* **98**, 9300–9305 (2001).
50. Wang, D. et al. Characterization of an MPS I-H knock-in mouse that carries a nonsense mutation analogous to the human IDUA-W402X mutation. *Mol. Genet. Metab.* **99**, 62–71 (2010).
51. Samaridou, E., Heyes, J. & Lutwyche, P. Lipid nanoparticles for nucleic acid delivery: current perspectives. *Adv. Drug Deliv. Rev.* **154–155**, 37–63 (2020).
52. Bennett, C. F. Therapeutic antisense oligonucleotides are coming of age. *Annu. Rev. Med.* **70**, 307–321 (2019).
53. Roberts, T. C., Langer, R. & Wood, M. J. A. Advances in oligonucleotide drug delivery. *Nat. Rev. Drug Discov.* **19**, 673–694 (2020).

Methods

Plasmid construction. For linear arRNA-expressing constructs, sequences of arRNAs were synthesized and Golden Gate cloned into the pLenti-sgRNA-lib 2.0 backbone (Addgene, no. 89638), with transcription of arRNA driven by either the hU6 or CMV promoter. For genetically encoded circ-arRNA-expressing constructs, we first constructed a cloning vector based on a pLenti-sgRNA-lib 2.0 vector that included a Twister P3 U2A, a 5′ ligation sequence, a 3′ ligation sequence and Twister P1 (ref. [36]). The sequences of arRNAs or random sequence nontargeting control RNAs were then synthesized and Golden Gate cloned into the autocatalytic circular RNA expression vector. The ribozyme mutation and deletion version precursor were constructed into the same backbone.

To increase editing efficiency further, circ-arRNA$_{151}$ was flanked by a 20-nt spacer and 30-nt polyAC sequences (AC50), then Golden Gate cloned into the genetically encoded circ-arRNA-expressing vector.

To reduce off-target editing, nucleotides opposite potential off-target adenosines were deleted and then cloned into the genetically encoded circ-arRNA-expressing vector.

To create the dual-fluorescence reporter, mCherry and eGFP coding sequences (the ATG start codon of eGFP was deleted) were PCR amplified and digested using BsmBI (Thermo Fisher Scientific, no. ER0452) before being subjected to T4 DNA ligase (NEB, no. M0202L)-mediated ligation with 3 × GGGGS linkers. The ligation product was subsequently inserted into the pLenti-CMV-MCS-PURO backbone.

To create constructs expressing genes with pathogenic mutations, full-length coding sequences of *TP53* (ordered from Vigenebio and donated by J. Wang's laboratory, Institute of Pathogen Biology, Chinese Academy of Medical Sciences) were amplified from constructs encoding the corresponding genes with the introduction of G-to-A mutations through mutagenesis PCR. Amplified products were cloned into the pLenti-CMV-MCS-mCherry backbone through the Gibson cloning method.

Gene vectors *ADAR1*^{p110}, *ADAR1*^{p150} and *ADAR2* were a gift from J. Han's laboratory, Xiamen University. These three genes were cloned into the pLenti-CMV-MCS-BSD backbone.

Cell line construction. To construct stable reporter cell lines, reporter constructs (pLenti-CMV-MCS-PURO backbone) were cotransfected into HEK293T cells together with two viral packaging plasmids, pR8.74 and pVSVG. After 72 h, viral supernatant was collected and stored at −80 °C. HEK293T cells were infected with lentivirus, and then mCherry$^+$ cells were sorted via fluorescence-activated cell sorting (FACS) and cultured to select a single clone cell line stably expressing a dual-fluorescence reporter system with no detectable eGFP background. Cell lines HEK293T *ADAR1*$^{-/-}$ and *TP53* $^{-/-}$ were generated according to a previously reported method[54]. ADAR1-targeting single-guide RNA and PCR-amplified donor DNA containing the CMV-driven puromycin resistance gene were cotransfected into HEK293T cells. Cells were then treated with puromycin 7 days after transfection. Single clones were isolated from puromycin-resistant cells and verified through sequencing and immunoblot analysis.

Production and purification of circRNAs in vitro. The production of circRNAs was performed according to previous reports. Briefly, circRNA precursors were synthesized via in vitro transcription (IVT) from linearized circRNA plasmid templates with a HiScribe T7 High Yield RNA Synthesis Kit (New England Biolabs, no. E2040S). After IVT, the IVT products were treated with DNase I (New England Biolabs, no. M0303S) for 30 min to digest DNA templates. For T4 RNA ligase circularization, either T4 RNA ligase 1 (New England Biolabs, no. M0239L) or T4 RNA ligase 2 (New England Biolabs, no. M0204L) was added to linear circRNA precursors and the mixture incubated at 37 °C overnight following DNase I digestion. For group I autocatalytic circularization, guanosine 5′-triphosphate was added to the reaction at a final concentration of 2 mM after DNase I digestion, then the reactions were incubated at 55 °C for 15 min to catalyze circRNA circularization. Cyclized circ-arRNAs were then column purified with a Monarch RNA Cleanup Kit (New England Biolabs, no. T2040L), and column-purified RNA was heated at 65 °C for 3 min and cooled on ice. The reactions were treated with RNase R (Epicentre, no. RNR07250) at 37 °C for 15 min to enrich circRNAs. RNase R-treated RNA was column purified.

To further enrich circ-arRNAs, purified RNase R-treated circ-arRNAs were resolved using HPLC (Agilent HPLC 1260) through a 4.6 × 300-mm^2 size-exclusion column with a particle size of 5 µm and pore size of 2,000 Å (Sepax Technologies, no. 215980P-4630) in RNase-free TE buffer using an Agilent HPLC 1260. Circ-arRNA-enriched fractions were collected and then column purified (New England Biolabs, no. T2040L). To further diminish the immunogenicity of purified circ-arRNAs, they were heated at 65 °C for 3 min, cooled on ice and subsequently treated with Quick CIP phosphatase (New England Biolabs, no. M0525S). Finally, circ-arRNAs were column purified and concentrated with an RNA Clean & Concentrator Kit (ZYMO, no. R1018).

Site-specific circRNA cleavage by RNaseH. Purified circ-arRNA and the same sequence precursor were proformed by RNaseH cleavage assay. Site-specific cleavage was performed in reactions containing 500 ng of target RNA, 50 pmol of the sense or antisense primer (Tsingke Biological Technology) and RNaseH buffer in a total volume of 18 µl. Reactions were incubated at 50 °C for 10 min followed by the addition of 2 µl of RNaseH (NEB, no. M0297L). Reactions proceeded for 2 h at 37 °C.

Cell culture and transfection. HeLa cells were obtained from Z. Jiang's laboratory (Peking University), and HEK293T cells were obtained from C. Zhang's laboratory (Peking University). A549 cells were obtained from EdiGene. C2C12 (ATCC, no. CRL-1772) cells were purchased from Procell. MEFs were generated from Idua-W392X mice. Hep G2 (ATCC, no. HB-8065)/RPE1 (ATCC, no. CRL-4000)/SF268 (NCI, no. 0502763)/COS-7 (ATCC, no. CRL-1651)/NIH3T3 (ATCC, no. CRL-1658) cells were maintained in our laboratory at Peking University. These mammalian cell lines were cultured in DBEM (Corning, no. 10-013-CV) with 10% fetal bovine serum supplemented with 1% penicillin–streptomycin under 5% CO_2 at 37 °C. Human primary hepatocytes (lonza, no. CC-3198) and cerebral organoids (HOPSTEM BIOTECH) were cultured according to the manufacturer's instructions.

Plasmids were transfected into cells with either X-tremeGENE HP DNA transfection reagent (Roche, no. 06366546001) or PEI (Proteintech, no. B600070), and RNAs cyclized in vitro were transfected into cells with Lipofectamine MessengerMax (Invitrogen, no. LMRNA003) according to the manufacturer's instructions.

RNA editing of exogenous transcripts. To assess RNA editing with the dual-fluorescence reporter system, HEK293T reporter cells were seeded in 12-well plates (~1–3 × 10^5 cells per well). After 24 h, cells were transfected with 2 µg of linear arRNA or circ-arRNA plasmids. Forty-eight hours after transfection, editing efficiency was assayed by quantification of the eGFP$^+$ ratio. ADAR1$^{-/-}$ HEK293T cells were transfected with reporter and linear arRNA or circ-arRNA plasmids as described for dual-fluorescence reporter cells.

To assess RNA editing efficiency in multiple cell lines, either 1 × 10^5 cells (HeLa, Hep G2, A549, RPE1, SF268, C2C12, NIH3T3, COS-7) or 4 × 10^5 cells (HEK293T) were seeded in 12-well plates. Twenty-four hours later, reporter and arRNA plasmids were transfected into these cells. Editing efficiency was assayed according to the protocol given in Supplementary Fig. 1d.

To evaluate the eGFP$^+$ ratio, cells were sorted and collected by FACS analysis 48 h post transfection. The mCherry signal served as a fluorescent selection marker for reporter/circ-arRNA-expressing cells, and percentages of eGFP$^+$/mCherry$^+$ cells were calculated as the readout for editing efficiency.

Separation of cytoplasm and nucleus. HEK293T cells were seeded in six-well plates (8 × 10^5 cells per well). Twenty-four hours later, cells were transfected with arRNA or circ-arRNA. Forty-eight hours post transfection, cells were collected and suspended in 200 µl of cytoplasmic lysis buffer containing 0.15% NP-40 (Thermo, no. FNN0021), 10 mM Tris HCl pH 7.0, 150 mM NaCl, Protease inhibitor (Roche, no. P8340) and RNase inhibitor (NEB, no. K1046) on ice. After 5 min, 500 µl of sacrose buffer containing 25% sacrose, 10 mM Tris HCl pH 7.0, 150 mM NaCl, Protease inhibitor (Roche, no. P8340) and RNase inhibitor (NEB, no. M0314L) was added slowly along the side wall. After centrifugation at 16,000*g* at 4 °C for 10 min, supernatant and sediment were separated as cytoplasmic and nucleic fractions, respectively. RNAs were isolated (Zymo, no. R1055) and reverse transcribed into complementary DNA with reverse-transcription PCR (RT–PCR).

RNA editing of endogenous transcripts. To assess RNA editing on endogenous mRNA transcripts, HEK293T cells were seeded in six-well plates (8 × 10^5 cells per well). Twenty-four hours later, cells were transfected with 4 µg of linear or circular arRNA plasmids. Forty-eight hours post transfection, cells were sorted and collected by FACS according to the protocol given in Supplementary Fig. 1d. For arRNAs targeting *KRAS* sites 3, 4 and 5, we collected total cells. RNA was isolated (Zymo, no. R1055) and reverse transcribed into cDNA via RT–PCR (Tiangen, no. KR118).

To assess RNA editing over a longer period of time, HEK293T cells were seeded in 12-well plates (4 × 10^5 cells per well). Twenty-four hours later, cells were transfected with 3 µg of linear or circular arRNA plasmids. To evaluate long-term RNA editing of arRNAs delivered by AAV, 1 × 10^5 HEK293T cells and 4 × 10^5 human primary hepatocytes were seeded in 24-well plates per well. Twenty-four hours later, cells were infected with AAV at a multiplicity of infection of either 1 × 10^6 (HEK293T, AAV9) or 5 × 10^5 (hepatocytes, AAV8). To further evaluate long-term RNA editing in organoids, cerebral organoids in 96-well plates were infected with 5 × 10^{11} genetic copies per well of AAV9 and then transferred to six-well plates 1 h after infection. Infected cerebral organoids were then cultured in a table concentrator at 66 r.p.m. Cells were collected at different time points and editing efficiency was assayed by NGS. Total RNA was isolated (Zymo, no. R1055) and reverse transcribed into cDNA via RT–PCR (TransGen Biotech, no. AH301).

The targeted locus was PCR amplified with the corresponding primers listed in Supplementary Table 2. PCR products were purified for Sanger sequencing or NGS (Illumina HiSeq X Ten).

RNA editing analysis of targeted sites. For NGS analysis, an index was generated using the targeted site sequences (20 nt upstream and downstream)

of arRNA-covered regions. Reads were aligned and quantified using Burrows–Wheeler aligner (v.0.7.10-r789). BAM alignment files were then sorted with SAMtools (v.1.1) and RNA editing sites were analyzed using REDitools (v.1.0.4). The parameters were as follows: -t 8 -U [AG] -n 0.0 -T 6-6 -e -d -u. All significant A-to-G conversions within the arRNA-targeted regions calculated by Fisher's exact test ($P < 0.05$) were considered edits made by arRNAs. Conversions at sites other than targeted adenosines were considered off-target edits. Mutations that appeared in the control and experimental groups simultaneously were considered to be due to single-nucleotide polymorphisms (SNPs).

Transcriptome-wide RNA sequencing analysis. Ctrl RNA_{151}- or circ-arRNA$_{151}$-*PPIA*-expressing plasmids with a blue fluorescent protein (BFP) expression cassette were transfected into HEK293T cells. BFP^+ cells were enriched by FACS 48 h after transfection, and RNA was purified with the RNAprep Pure Micro Kit (Tiangen, no. DP420). mRNA was then purified using an NEBNext Poly(A) mRNA Magnetic Isolation Module (New England Biolabs, no. E7490), processed with an NEBNext Ultra II RNA Library Prep Kit for Illumina (New England Biolabs, no. E7770) and subjected to NGS analysis using an Illumina HiSeq X Ten platform (2 × 150-base pair (bp) paired-end reads; 30 Gb for each sample). To exclude nonspecific effects caused by transfection, we included a mock group in which we treated cells with transfection reagent only. Each group contained four replicates.

The bioinformatics analysis pipeline followed the work of Vogel et al.[13]. Quality control was conducted using FastQC (v.0.11.8), and quality trimming was performed with Cutadapt (v.1.16; the first 6 bp of each read were trimmed, and up to 20 bp quality trimmed). AWK scripts were used to filter out the introduced circ-arRNAs. After trimming, reads of length <90 nt were filtered out. Subsequently, filtered reads were mapped to the reference genome (GRCh38-hg38) by STAR software (v.2.6.1b). We used the GATK HaplotypeCaller (v.4.0.7.0) to call variants. The raw variant call format files generated with GATK (v.4.0.7.0) were filtered and annotated with GATK VariantFiltration (v.4.0.7.0), bcftools (v.1.9) and ANNOVAR. Variants in dbSNP, the 1000 Genomes Project database and EVS were filtered out. Shared variants in six replicates of each group were then selected as RNA editing sites. For SNP filtration, GATK (v.4.0.7.0) parameters were set as follows: *QD < 2.0, FS > 60, MQ < 30, MQRankSum < −12.5, ReadPosRankSum < −8.0, DP < 20.0, QUAL < 20.0*. The RNA editing level of the mock group was viewed as the background, and the global targets of Ctrl RNA_{151} and circ-arRNA$_{151}$-*PPIA* were obtained by subtracting variants in the mock group.

RNA-seq data were analyzed for interrogation of possible transcriptional changes induced by RNA editing events. Analysis of transcriptome-wide gene expression was performed using HISAT2 (v.2.1.0) and STRINGTIE (v.1.3.5) software. We used Cutadapt (v.1.16) and FastQC (v.0.11.8) for quality control of sequencing data. Sequencing reads were then mapped to the reference genome (GRCh38-hg38) using HISAT2 (v.2.1.0), followed by Pearson's correlation coefficient analysis as mentioned above. FPKM values were calculated with STRINGTIE (v.1.3.5).

To assess whether circ-arRNAs perturb natural editing homeostasis, we analyzed global editing sites shared by the Ctrl RNA_{151} and circ-arRNA$_{151}$-*PPIA* groups. Differential RNA editing rates at native A-to-I editing sites were assessed using Pearson's correlation coefficient analysis.

Assay of activation of *CTNNB1*. To evaluate activation of the Wnt signaling pathway, HEK293T cells were seeded in 12-well plates (4×10^5 cells per well). Twenty-four hours later, cells were transfected with 2 μg of linear or circular arRNA plasmids targeting the transcripts of *CTNNB1* (T41), 500 ng of TOPFlash (beyotime, no. D2501) or FOPFlash (beyotime, no. D2503) and 25 ng of Renilla luciferase. Total cells were collected and assayed using the Promega Dual-Glo Luciferase Assay System (Promega, no. E2940) according to the manufacturer's protocol 72 h post transfection. The TOPFlash reporter provides a metric of β-catenin activation when compared to the background as measured by the FOPFlash reporter under the same condition. The accumulated β-catenin activated the TOPFlash reporter by binding the promoter region but not the FOPFlash reporter, which contains a mutation on the promoter region. Folding activation was calculated by taking the ratio of the average TOPFlash measurement divided by the average FOPFlash measurement.

Assay of transcriptional regulatory activity of p53. *$TP53^{W53X}$* cDNA-expressing plasmids and circ-arRNA-expressing plasmids were transfected into HEK293T *$TP53^{-/-}$* cells, together with p53-firefly luciferase *cis*-reporting plasmids (YRGene, no. VXS0446) and Renilla luciferase plasmids (gifts from Z. Jiang's laboratory, Peking University) to detect the transcriptional regulatory activity of p53. Forty-eight hours after transfection, cells were collected and assayed with a Promega Dual-Glo Luciferase Assay System (Promega, no. E2940) according to the manufacturer's protocol. Luminescence was measured by an Infinite M200 reader (Tecan). Fold change in p53-induced luciferase activity was calculated as the ratio of firefly luminescence to Renilla luminescence.

Immunoblot analysis. We used mouse monoclonal primary antibodies against p53 (Santa Cruz, no. sc-126), anti-cyclophilin A antibody (abcam, no. ab58144) and β-tubulin (CWBiotech, no. CW0098). A horseradish-peroxidase-conjugated goat anti-mouse IgG secondary antibody (H + L, no. 115-035-003) was purchased from Jackson ImmunoResearch. Next, 2×10^6 cells were sorted for lysis and an equal amount of protein from each lysate was loaded for SDS–PAGE, then sample proteins were transferred to polyvinylidene difluoride membranes (Bio-Rad Laboratories). Membranes were immunoblotted with primary antibodies (anti-p53, 1:300; anti-cyclophilin A, 1:1,000; anti-tubulin, 1:2,000), incubated with a secondary antibody (1:3,000) and exposed. The experiments were repeated three times. Semiquantitative analysis was performed with Image Lab software.

Cytokine expression assay and ADAR relative quantification. HEK293T cells were seeded on 12-well plates (4×10^5 cells per well). When approximately 70% confluent, cells were transfected with 3 μg of circ-arRNA. As a positive control, 1 μg of poly (I:C) (Invitrogen, tlrl-picw) was transfected. Forty-eight hours later, cells were collected and subjected to RNA isolation (Zymo, no. R1055). Then, total RNAs were reverse transcribed into cDNA via RT–PCR (TIANGEN, no. KR103-04) and expression levels of *RIG-I*, *MDA5*, *OAS1*, *OASL*, *PKR*, *IFN-β*, *ISG56*, *IL-6*, *IL-8*, *RANTES*, *IL-12*, *IL-1β*, *MCP1*, *MIP1A*, *IL10*, *$ADAR1^{p110}$*, *$ADAR1^{p150}$* and *ADAR2* were measured by qPCR (TAKARA, no. RR820A). Primer sequences are listed in Supplementary Table 2.

Animal experiments. The experimental animals included 4- or 6-week-old Idua-W392X (B6.129S-*$Idua^{tm1.1Kmke}$*/J) female mice (Jackson Laboratory, no. 017681) and C57BL/6 J female mice (Beijing Vital River Laboratory). Mice were housed at 18–23 °C with 40–60% humidity under a normal 12/12-h light/dark cycle with food and water available ad libitum under specific-pathogen-free conditions in the Laboratory Animal Center of Peking University. The animal experiments were approved by Peking University Laboratory Animal Center (Beijing) and undertaken in accordance with the National Institutes of Health Guide for Care and Use of Laboratory Animals.

Circ-arRNAs were packaged in AAV8 by PackGene Biotech. The AAV titer was 1×10^{13} virus/200 μl; 200 μl of AAV was injected into the tail vein of each IDUA-W392X mouse. Mice were monitored four times per week for the duration of the experiment (4 weeks).

Harvested mouse tissues were homogenized in 1 ml of TRIzol, and RNA was extracted by the chloroform extraction method. Tissue RNA was then reverse transcribed, PCR amplified and analyzed by Sanger sequencing or NGS. Four or six independent biological replicates were performed in each experiment.

IDUA catalytic activity assay. Gathered cell pellets were resuspended and lysed with 28 μl of 0.5% Triton X-100 in 1 × PBS buffer on ice for 30 min. Then, 25 μl of cell lysate was added to 25 μl of 190 μM 4-methylumbelliferyl-α-l-iduronidase substrate (Cayman, no. 2A-19543-500), which was dissolved in 0.4 M sodium formate buffer containing 0.2% Triton X-100 (pH 3.5) and incubated for 90 min at 37 °C in the dark. The catalytic reaction was quenched by the addition of 200 μl of 0.5 M NaOH/glycine buffer (pH 10.3) and then centrifuged for 2 min at 4 °C. The supernatant was transferred to a 96-well plate, and fluorescence was measured at 365-nm excitation wavelength and 450-nm emission wavelength with an Infinite M200 reader (Tecan). The standard curve generated used pure end product (4-methylumbelliferone).

Measurement of tissue GAG. The GAG content of liver tissue were measured using the Blyscan GAG assay kit (Blyscan, no. B1000): 50 mg of liver tissue was digested with 1 ml of papain extraction reagent at 65 °C for 3 h. Supernatant GAG content was assayed according to the manufacturer's protocol.

Statistics and reproducibility. The number of independent experiments performed in parallel is represented by *n*. Unpaired two-tailed Student's *t*-test was implemented for group comparisons as indicated in the figure legends. $^*P < 0.05$, $^{**}P < 0.01$, $^{***}P < 0.001$, $^{****}P < 0.0001$. Three independent experiments were performed in Figs. 1e, 3b and 4e and Supplementary Figs. 2e, 5b and 10a, with similar results. For transcriptome-wide RNA-seq analysis, two independent experiments were performed in $ADAR2_{DD}$ overexpression groups; six and three independent experiments were performed in cells transfected by circ-arRNA$_{151}$ and Ctrl RNA_{151}, respectively.

Reporting Summary. Further information on research design is available in the Nature Research Reporting Summary linked to this article.

Data availability

All data and materials presented in this manuscript are available from the corresponding author (W.W.) upon reasonable request with a completed material transfer agreement. Raw data for whole-transcriptome RNA-seq are available as a BioProject with Project ID PRJNA775856. Source data are provided with this paper.

References

54. Zhou, Y., Zhang, H. & Wei, W. Simultaneous generation of multi-gene knockouts in human cells. *FEBS Lett.* **590**, 4343–4353 (2016).

Acknowledgements

We thank the staff of the BIOPIC High-throughput Sequencing Center (Peking University) and Genetron Health for their assistance in NGS analysis, and the National Center for Protein Sciences (Beijing) and the flow cytometry Core at National Center for Protein Sciences at Peking University, particularly Y. Guo and F. Wang, for technical help. We thank the High-Performance Computing Platform at Peking University for providing the platforms for NGS data analysis. We thank the Laboratory Animal Center at Peking University for the feeding of mice. This project was supported by funds from the National Key R&D Program of China (no. 2020YFA0707800), the Beijing Municipal Science & Technology Commission (no. Z181100001318009), the National Science Foundation of China (no. 31930016), the Beijing Advanced Innovation Center for Genomics at Peking University and the Peking-Tsinghua Center for Life Sciences (both to W.W.) and the Fellowship of China National Postdoctoral Program for Innovative Talents (no. BX20200010 to L.Q.).

Author contributions

W.W. conceived and supervised this project. W.W., Z.Y., L.Q. and H.T. designed experiments. Z.Y., L.Q. and H.T. performed experiments with the help of P.Y., Z.Y., Y.Z., X.Z., Z.F., F.T. and C.W. Y.Y. conducted all sample preparation for NGS. Z.Y., Z.L. and Y.L. performed data analysis. Z.Y., L.Q. and W.W. wrote the manuscript with help from the other authors.

Competing interests

Two patents have been filed relating to the data presented. W.W., Z.Y., L.Q., F.T. and C.W. are coinventors on patent applications describing circ-arRNA. W.W. and Z.Y. are coinventors on patent applications describing engineered circ-arRNA. P.Y., Z.Y. and Y.Z. are employees of EdiGene Inc. W.W. is a founder and scientific adviser for EdiGene, Inc. The other authors declare no competing interests.

Additional information

Supplementary information The online version contains supplementary material available at https://doi.org/10.1038/s41587-021-01180-3.

Correspondence and requests for materials should be addressed to Wensheng Wei.

Peer review information *Nature Biotechnology* thanks Michael Jantsch and the other, anonymous, reviewer(s) for their contribution to the peer review of this work.

Reprints and permissions information is available at www.nature.com/reprints.

nature research

Corresponding author(s): Wensheng Wei

Last updated by author(s): Nov 16, 2021

Reporting Summary

Nature Research wishes to improve the reproducibility of the work that we publish. This form provides structure for consistency and transparency in reporting. For further information on Nature Research policies, see our Editorial Policies and the Editorial Policy Checklist.

Statistics

For all statistical analyses, confirm that the following items are present in the figure legend, table legend, main text, or Methods section.

n/a	Confirmed	
☐	☒	The exact sample size (*n*) for each experimental group/condition, given as a discrete number and unit of measurement
☐	☒	A statement on whether measurements were taken from distinct samples or whether the same sample was measured repeatedly
☐	☒	The statistical test(s) used AND whether they are one- or two-sided *Only common tests should be described solely by name; describe more complex techniques in the Methods section.*
☒	☐	A description of all covariates tested
☐	☒	A description of any assumptions or corrections, such as tests of normality and adjustment for multiple comparisons
☐	☒	A full description of the statistical parameters including central tendency (e.g. means) or other basic estimates (e.g. regression coefficient) AND variation (e.g. standard deviation) or associated estimates of uncertainty (e.g. confidence intervals)
☐	☒	For null hypothesis testing, the test statistic (e.g. *F*, *t*, *r*) with confidence intervals, effect sizes, degrees of freedom and *P* value noted *Give P values as exact values whenever suitable.*
☒	☐	For Bayesian analysis, information on the choice of priors and Markov chain Monte Carlo settings
☒	☐	For hierarchical and complex designs, identification of the appropriate level for tests and full reporting of outcomes
☐	☒	Estimates of effect sizes (e.g. Cohen's *d*, Pearson's *r*), indicating how they were calculated

Our web collection on statistics for biologists contains articles on many of the points above.

Software and code

Policy information about availability of computer code

Data collection	No software was used.
Data analysis	REDitools (v1.0.4) was used for targeted RNA editing analysis. FastQC (v.0.11.8), Cutadapt (v.1.16), STAR (v.2.6.1b), GATK Haplotypcaller (v.4.0.7.0), GATK VariantFiltration (v.4.0.7.0), bcftools (v1.9), ANNOVAR, HISAT2 (v.2.1.0) and STRINGTIE (v.1.3.5) were adopted for transcriptome-wide RNA-sequencing analysis. The minimum free energy of double-stranded RNA was predicted by RNAhybrid. R script was used for ploting figure. GraphPad Prism 8 was used for basic statistical analysis and graph production.

For manuscripts utilizing custom algorithms or software that are central to the research but not yet described in published literature, software must be made available to editors and reviewers. We strongly encourage code deposition in a community repository (e.g. GitHub). See the Nature Research guidelines for submitting code & software for further information.

Data

Policy information about availability of data

All manuscripts must include a data availability statement. This statement should provide the following information, where applicable:

- Accession codes, unique identifiers, or web links for publicly available datasets
- A list of figures that have associated raw data
- A description of any restrictions on data availability

All data and materials presented in this manuscript are available from the corresponding author (W.W.) upon reasonable request with a completed Material Transfer Agreement. Raw data of whole transcriptome RNA-seq is available as a BioProject with Project ID PRJNA775856.

Field-specific reporting

Please select the one below that is the best fit for your research. If you are not sure, read the appropriate sections before making your selection.

☒ Life sciences ☐ Behavioural & social sciences ☐ Ecological, evolutionary & environmental sciences

For a reference copy of the document with all sections, see nature.com/documents/nr-reporting-summary-flat.pdf

Life sciences study design

All studies must disclose on these points even when the disclosure is negative.

Sample size	In this study, targeted RNA editing of reporter transcripts or endogenous transcripts was done with independent experiments performed in parallel, and the number of replicates was listed in the text and figure legends. Numbers of independent experiments performed in transcriptome-wide RNA-sequencing analysis were described in Statistics and Reproducibility. Three independent experiments were performed with similar results in Image, Western blot and agarose electrophoresis.
Data exclusions	No data were excluded.
Replication	The numble of replications is always mentioned in text, methods and figure legends. All attempts at replication were successful.
Randomization	During FACS experiments for sorting transfected cells, all the cells were transfected and sorted via FACS according to the corresponding fluorescence maker, and untreated group and mock group (fluorescence-negative) were conducted for gating.
Blinding	No blinding was performed due to the involvement of several experimentators.

Reporting for specific materials, systems and methods

We require information from authors about some types of materials, experimental systems and methods used in many studies. Here, indicate whether each material, system or method listed is relevant to your study. If you are not sure if a list item applies to your research, read the appropriate section before selecting a response.

Materials & experimental systems

n/a	Involved in the study
☐	☒ Antibodies
☐	☒ Eukaryotic cell lines
☒	☐ Palaeontology and archaeology
☐	☒ Animals and other organisms
☒	☐ Human research participants
☒	☐ Clinical data
☒	☐ Dual use research of concern

Methods

n/a	Involved in the study
☒	☐ ChIP-seq
☐	☒ Flow cytometry
☒	☐ MRI-based neuroimaging

Antibodies

Antibodies used	Anti-p53 antibody (Santa Cruz, sc-126) ;Anti-beta-tubulin antibody (CWBiotech, CW0098); Anti-Cyclophilin A antibody (abcam, ab58144).
Validation	All antibodies used in this study were validated by the manufacturer, and the western blot experiments were performed according to the manufacturer's instruction. And the western blot data were provided in the manuscript.

Eukaryotic cell lines

Policy information about cell lines

Cell line source(s)	HeLa cells were obtained from Z. Jiang's laboratory (Peking University). And HEK293T cells were obtained from C. Zhang's laboratory (Peking University). A549 cells were obtained from EdiGene. C2C12 (ATCC, CRL-1772) cells were purchased from Procell. MEFs were generated from IduaW392X mice. Hep G2 (ATCC, HB-8065) /RPE1 (ATCC , CRL-4000) /SF268 (NCI, 0502763) /COS-7 (ATCC , CRL-1651) /NIH3T3 (ATCC , CRL-1658) cells were maintained in our laboratory at Peking University.
Authentication	STR analysis was used for cell line authentication.
Mycoplasma contamination	All cells were tested negative for mycoplasma contamination.

Commonly misidentified lines (See ICLAC register)	No commonly misidentified cell lines were used.

Animals and other organisms

Policy information about studies involving animals; ARRIVE guidelines recommended for reporting animal research

Laboratory animals	The experimental animals included 4- or 6-week-old Idua-W392X (B6.129S-Iduatm1.1Kmke/J) female mice (Jackson Laboratory) and C57BL/6J female mice (Beijing Vital River Laboratory). Mice were housed at 18–23 °C with 40–60% humidity under a normal 12-h light–dark cycle with food and water available ad libitum under SPF (specific pathogen-free) conditions in the Laboratory Animal Center of Peking University.
Wild animals	This study did not involve wild animals.
Field-collected samples	This study did not involve field-collected samples.
Ethics oversight	The animal experiments were approved by Peking University Laboratory Animal Center (Beijing). All experiment protocols were approved by the respective Laboratory Animal Care and Use Committees of Peking University, and undertaken in accordance with the National Institute of Health Guide for Care and Use of Laboratory Animals.

Note that full information on the approval of the study protocol must also be provided in the manuscript.

Flow Cytometry

Plots

Confirm that:

☒ The axis labels state the marker and fluorochrome used (e.g. CD4-FITC).

☒ The axis scales are clearly visible. Include numbers along axes only for bottom left plot of group (a 'group' is an analysis of identical markers).

☒ All plots are contour plots with outliers or pseudocolor plots.

☒ A numerical value for number of cells or percentage (with statistics) is provided.

Methodology

Sample preparation	Cells were transfected using the X-tremeGENE HP DNA transfection reagent (06366546001; Roche, Mannheim, German) or PEI (Proteintech, B600070) according to the supplier's protocols. About 48 to 72 hours later, cells were digested with trypsin and collected for the following FACS according to the fluorescence maker (mCherry, EGFP or BFP).
Instrument	BD Aria SORP and BD LSRFortessa SORP
Software	BD FACSDiva
Cell population abundance	The fluorescence maker was encoded in the expression plasmids for sorting transfected cells, and about 1×10^6 cells were collected for further process.
Gating strategy	Firstly, the starting cell population were selected according to SSC-A, FSC-A, SSC-W and SSC-H gates. Then fluorescence-positive cell population were determined according to the fluorescence-negative population control (untreated group).

☐ Tick this box to confirm that a figure exemplifying the gating strategy is provided in the Supplementary Information.